# Is Bursting More Effective than Spiking in Evoking Pituitary Hormone Secretion? A Spatiotemporal Simulation Study of Calcium and Granule Dynamics

Alessia Tagliavini[1], Joël Tabak[2,3], Richard Bertram[2], Morten Gram Pedersen[1]

[1] Department of Information Engineering, University of Padua, Padua, Italy

[2] Department of Mathematics and Program in Neuroscience and Molecular Biophysics, Florida State University, Tallahassee, FL 32306, USA

[3] Exeter University Medical School, Biomedical Neuroscience, Exeter, UK

Corresponding author:

Morten Gram Pedersen,

Department of Information Engineering, University of Padua,

Via Gradenigo 6/B, 35131 Padua, Italy.

Email: pedersen@dei.unipd.it

Running head:

Pituitary secretion evoked by bursting and spiking

Author contributions:

Conceived research: RB, MGP

Performed research: AT, JT

Prepared figures: AT

Wrote and edited manuscript, and approved final version: AT, JT, RB, MGP

Keywords: electrical activity; exocytosis; $Ca^{2+}$ oscillations; mathematical modeling; dynamic clamp.

## ABSTRACT

Endocrine cells of the pituitary gland secrete a number of hormones, and the amount of hormone released by a cell is controlled in large part by the cell's electrical activity and subsequent $Ca^{2+}$ influx. Typical electrical behaviors of pituitary cells include continuous spiking and so-called pseudo-plateau bursting. It has been shown that the amplitude of $Ca^{2+}$ fluctuations is greater in bursting cells, leading to the hypothesis that bursting cells release more hormone than spiking cells. In this work, we apply computer simulations to test this hypothesis. We use experimental recordings of electrical activity as input to mathematical models of $Ca^{2+}$ channel activity, buffered $Ca^{2+}$ diffusion, and $Ca^{2+}$-driven exocytosis. To compare the efficacy of spiking and bursting on the same cell, we pharmacologically block the large conductance potassium (BK) current from a bursting cell, or add a BK current to a spiking cell via dynamic clamp. We find that bursting is generally at least as effective as spiking at evoking hormone release, and is often considerably more effective, even when normalizing to $Ca^{2+}$ influx. Our hybrid experimental/modeling approach confirms that adding a BK-type $K^+$ current, which is typically associated with decreased cell activity and reduced secretion, can actually produce an increase in hormone secretion, as suggested earlier.

## INTRODUCTION

Endocrine cells of the pituitary gland (i.e., melanotrophs, lactotrophs, somatotrophs, thyrotrophs, corticotrophs, and gonadotrophs) secrete a number of hormones and are regulated by the hypothalamus (30). These hormones act on other endocrine glands and other tissues including the brain to regulate physiological and behavioral aspects of growth, metabolism, water balance, and reproduction (7). The endocrine pituitary cells contain a wide variety of ion channels and are electrically excitable, and hormone secretion occurs due to an elevation in the intracellular $Ca^{2+}$ concentration that often accompanies electrical activity (29). Common behaviors of the cells include continuous spiking – typically observed in luteinizing hormone-secreting gonadotrophs under basal conditions – and a form of bursting known as pseudo-plateau bursting often observed in prolactin-secreting lactotrophs, growth hormone-releasing somatotrophs, and ACTH-secreting corticotrophs, where the burst duration is at most a few seconds and the spikes that ride on the elevated voltage plateau are very small (9, 10). Each electrical event brings $Ca^{2+}$ into the cell, and this $Ca^{2+}$ is responsible for exocytosis of hormone-filled granules. Simultaneous measurements of both electrical activity and $Ca^{2+}$ concentration have established that the amplitude of $Ca^{2+}$ fluctuations is greater in a bursting cell than in a spiking cell (30) leading to the hypothesis that bursting cells release more hormone than spiking cells (8, 9). Experimentally exploring this hypothesis will require simultaneous measurements of electrical activity and release from single cells. The aim of this report is to use computer simulations to explore the hypothesis that pseudo-plateau bursting evokes more secretion than continuous spiking.

The approach that we use is to directly measure electrical spiking and bursting patterns from pituitary cells and use these data as input to mathematical models of $Ca^{2+}$ channel activity, $Ca^{2+}$ diffusion and binding to buffer, and finally $Ca^{2+}$-driven exocytosis. The model parameters are set according to prior data and models, but one major unknown factor is the geometrical arrangement of $Ca^{2+}$ channels and docked granules at the plasma membrane. We consider the secretion response to stochastic single channels as well as small clusters of stochastic channels, and vary the distance of the channels from the release sites. Our objective is to determine how these factors affect the differential secretion evoked by spiking electrical activity vs. bursting electrical activity.

We find that bursting is typically more effective at evoking secretion than is continuous spiking. When bursting is induced in a spiking gonadotroph by injecting a BK-type $K^+$ current with dynamic clamp, our model simulations suggest that the burst pattern is generally at least as effective as continuous spiking at evoking hormone release, and is often considerably more effective. We demonstrate that the degree of superiority of bursting over spiking depends on the channel configuration, which would likely vary from cell-to-cell. We also demonstrate that the bursting reappearing in an endogenously bursting pituitary cell, after previously pharmacologically blocking the native BK current and subsequently adding a BK current using dynamic clamp, is superior at evoking secretion than the pharmacologically induced spiking behavior. Thus, we demonstrate with this hybrid experimental/modeling approach that adding a $K^+$ current, which is typically associated with decreased cell activity and reduced secretion, can actually produce an increase in hormone secretion, as suggested earlier (9).

## METHODS

The inputs to our mathematical models are voltage time courses recorded from a rat gonadotroph or from a GH4C1 lacto-somatotroph cell. We use traces consisting of continuous spiking patterns, and traces of fast pseudo-plateau bursting caused by adding a BK-type current to a spiking cell with the dynamic clamp technique. Each of these traces is fed into a mathematical model consisting of stochastic $Ca^{2+}$ channels coupled to reaction-diffusion equations that describe $Ca^{2+}$ transport through the cell. Finally, the computed $Ca^{2+}$ concentration is used to drive an exocytosis model based on $Ca^{2+}$ binding to granules, granule fusion with the membrane, and resulting hormone release.

### EXPERIMENTAL

GH4C1 cells were maintained in culture conditions in supplemented F10 medium (Sigma-Aldrich, St-Louis, MO) according to established procedures (35). Primary pituitary cells were obtained from diestrous female rats (Sprague Dawley, aged 3-6 months) using enzymatic dispersion of pituitary fragments (33). Animal procedures were approved by the Florida State

University Animal Care and Use Committee. Cells were cultured in supplemented M199 medium (Invitrogen, Carlsbad, CA) for one day before being used for patch clamp experiments. Gonadotrophs were identified by their larger size and by their typical rhythmic hyperpolarizations in response to 1 nM gonadotropin-releasing hormone (Bachem, Torrance, CA) applied at the end of the experiment (38).

During the patch-clamp experiments, cells were superfused with Hepes-buffered saline (138 mM NaCl, 5mM KCl, 10 mM D-glucose, 25 mM HEPES, 0.7 mM $Na_2HPO_4$, 1 mM $MgCl_2$, 2 mM $CaCl_2$) at room temperature. Patch pipettes (resistance 6-9 MOhm) were filled with solution containing 90 mM KAsp, 60 mM KCl, 10 mM HEPES, 1 mM $MgCl_2$ with the addition of 120 g/ml amphotericin B. Usually, access resistance decreased below 50 MOhm within 10 minutes following seal (> 5 GOhm) formation. BK channels were blocked by bath application of 100 nM iberiotoxin (Tocris).

## DYNAMIC CLAMP

Membrane potential was recorded in current clamp (bridge mode) and output from the patch amplifier (Multiclamp 700B, Molecular Devices, Sunnyvale, CA) was read through an analog to digital acquisition card (DAQ) on a PC running the software QuB with a dynamic clamp module (22). Membrane potential ($V$) was used to compute the current going through the BK channels, $I_{BK} = g_{BK} f (V_K - V)$, with $f$ obtained by integrating

$$\tau_{BK} \frac{df}{dt} = f_\infty(V) - f$$

in real time using the forward Euler method (22), with $dt$ average = 54 μs, maximum = 100 μs, and the steady state BK channel activation given by

$$f_\infty(V) = \left[1 + \exp\left((v_f - V)/s_f\right)\right]^{-1} .$$

The calculated BK current was injected back into the cell through the same DAQ. The parameter values were: $g_{BK}$ = 0.5 – 1 nS; $\tau_{BK}$ = 5 – 10 ms; $v_f$ = -15 mV; $s_f$ = 1 mV.

## MODELLING

### GEOMETRY

To model data from pituitary cells we represented a single cell by a sphere with a diameter of 13 μm (5). Based on whole-cell calcium conductance of ~1.5-2 nS (10), and single channel conductance ~20 pS (13), we assumed that a cell possesses 75 functional L-type $Ca^{2+}$ channels. In our simulations we considered two different configurations for the channel distribution over the sphere surface: channels were either uniformly distributed and each release site affected by a single channel, or there were clusters composed of 5 channels, and each release site affected by a single cluster. In the single channel case, $Ca^{2+}$ diffusion was computed in a conical region with base radius of 1.5 μm (Fig. 1a), a radius obtained by dividing the sphere surface into 75 circular areas, one for each channel. This radius corresponds to an inter-channel distance of ~3 μm, in agreement with (11). The single channel conductance was set to 20 pS (13). In the case of channel clusters, $Ca^{2+}$ diffusion was simulated in a conical region with a base radius of 3.3 μm, corresponding to dividing the sphere surface into 15 circular areas. In both cases, the $Ca^{2+}$ current source was located at the base center of the conical region. We implemented no-flux boundary conditions for $Ca^{2+}$ and buffers on the sides of the cone. This assumption means that $Ca^{2+}$ flowing out of the conical region equals the flux into the cone from adjacent regions, or in other words, that the $Ca^{2+}$ channels in adjacent cones contribute to $Ca^{2+}$ levels in the cone of study exactly as the $Ca^{2+}$ channel or cluster under study influences the adjacent regions. Because of the conical geometry, the full 3-dimensional problem was reduced to a 2-dimensional problem, using rotationally symmetric spherical $(r,\theta)$ coordinates, thus reducing the computational requirements. Since the granules participating in hormone secretion are located just below the membrane (14), we focused our attention on the submembrane $Ca^{2+}$ profiles along the plasma membrane.

[Figure 1]

158 SINGLE CHANNEL CURRENT

159 For the single $Ca^{2+}$ channel, we assumed three states with kinetic mechanism described
160 by (28)

$$C \underset{\beta}{\overset{\alpha}{\rightleftharpoons}} O \underset{k_-}{\overset{k_+}{\rightleftharpoons}} B, \tag{1}$$

161 where the states are closed ($C$), open ($O$), and blocked or inactivated ($B$).

162 The rate constants $\alpha(V)$ and $\beta(V)$ were determined by $\alpha=m_\infty/\tau_m$ , $\beta=1/\tau_m - \alpha$ (12) using a steady-
163 state activation function $m_\infty$ and time constant $\tau_m$ obtained from experiments. Based on data from
164 GH3 cells (5, 11), which have $Ca^{2+}$ channel characteristics similar to GH4 cells (5), and in
165 agreement with Sherman et al. (28), we set $\tau_m$=1.25 ms. The steady-state activation function was

$$m_\infty = \frac{1}{1+\exp[(V_m - V)/s_m]}, \tag{2}$$

166 with $V_m$ = –4 mV and $s_m$ = 7 mV (11). With regards to channel inactivation, some types of $Ca^{2+}$
167 channels are inactivated by $Ca^{2+}$, while others exhibit voltage-dependent inactivation. We found
168 that fixed rate constants $k_-$=0.018 $ms^{-1}$ and $k_+$=0.0324 $ms^{-1}$ were sufficient to match inactivation
169 experimentally observed in (11). The stochastic channel dynamics (1) was simulated as
170 realizations of the discrete-state continuous-time Markov chain with transition probabilities for a
171 small time step $\Delta t$ described by

$$\begin{bmatrix} O(t+\Delta t) \\ C(t+\Delta t) \\ B(t+\Delta t) \end{bmatrix} = \begin{bmatrix} 1-(\beta+k_+)\Delta t & \alpha\Delta t & k_-\Delta t \\ \beta\Delta t & 1-\alpha\Delta t & 0 \\ k_+\Delta t & 0 & 1-k_-\Delta t \end{bmatrix} \begin{bmatrix} O(t) \\ C(t) \\ B(t) \end{bmatrix}. \tag{3}$$

Monte Carlo simulations were performed and the single-channel open-state $O(t)$ was used to compute the single-channel current as

$$I_{sc}(t) = g_{sc} O(t)(V(t) - V_{Ca}) \tag{4}$$

where $g_{sc}$ is the single channel conductance. In the cluster case, the total current is simulated by summing 5 independent realizations of a single channel current ($I_{sc}$). Both the current driving force and open probability are coupled to the time-varying membrane potential $V(t)$. Specifically, the driving force decreases as $V(t)$ increases towards the $Ca^{2+}$ reversal potential $V_{Ca}$ whereas the open probability increases with $V(t)$.

## ENDOGENOUS BUFFERS

In all simulations we assumed the presence of a single immobile endogenous $Ca^{2+}$ buffer, in agreement with Kits et al. (15), and no mobile buffers were considered. Binding of $Ca^{2+}$ to the buffers is described by simple mass action kinetics with one-to-one stoichiometry,

$$B + Ca^{2+} \underset{k_{off}}{\overset{k_{on}}{\rightleftharpoons}} CaB, \tag{5}$$

where $k_{on}$ and $k_{off}$ are association and disassociation rates, respectively. The reaction-diffusion equations for the $Ca^{2+}$ concentration and for the free unbound buffers are taken from (20):

$$\begin{aligned}\frac{\partial [Ca^{2+}]}{\partial t} = {} & D_{Ca}\nabla^2\left[Ca^{2+}\right] - k_{on}\left[Ca^{2+}\right][B] + k_{off}\left(B_{total} - [B]\right) + \frac{1}{2F} I_{sc}(t)\delta(r - R, \theta) \\ & - k_{uptake}\left(\left[Ca^{2+}\right] - \left[Ca^{2+}\right]_0\right),\end{aligned} \tag{6}$$

$$\frac{\partial [B]}{\partial t} = -k_{on}\left[Ca^{2+}\right][B] + k_{off}\left(B_{total} - [B]\right), \tag{7}$$

where $D_{Ca}$ is the diffusion coefficient for unbound $Ca^{2+}$. We chose $D_{Ca}$=0.2 μm$^2$ ms$^{-1}$ (1) and assumed that the distribution of the immobile buffer is spatially uniform. The second-to-last term in Eq. 6 represents $Ca^{2+}$ influx, where $F$ is Faraday's constant, $I_{sc}(t)$ is the (inward) single-channel (or 5-channel-cluster) calcium current, and $\delta(r\text{-}R,\theta)$ is the Dirac delta function centered at $r$=$R$ and $\theta$=0 (i.e., at the center of the base of the cone). The last term defines net $Ca^{2+}$ uptake into internal stores such as the endoplasmic reticulum with constant rate $k_{uptake}$ =0.3 μM/ms$^{-1}$. $[Ca^{2+}]_0$ is the $Ca^{2+}$ concentration in case of no $Ca^{2+}$ influx and spatiotemporal equilibrium. In accordance with simulation studies performed by Kits et al. (16) in melanotroph cells, we set the endogenous buffer parameters $k_{on}$=0.1 μM$^{-1}$ ms$^{-1}$, $K_D$= $k_{off}/k_{on}$ =10 μM, and $B_{total}$=900 μM. No-flux boundary conditions hold for $Ca^{2+}$ at all boundaries. The reaction-diffusion equations were solved using the Calcium Calculator (CalC) software developed by Victor Matveev (21). CalC uses an alternating-direction implicit finite difference method, with second order accuracy in space and time, and with adaptive time steps.

## EXOCYTOSIS MODEL

We initially used a 6-pool exocytosis model (4), which describes the fraction of granules in various pools of granules described as docked, primed, domain bound, or in one of three pre-fusion states distinguished by the number of bound $Ca^{2+}$ ions. However, for the relatively short time courses used here (5 sec), our preliminary simulations showed no significant differences between this 6-pool model and a simpler 4-pool model in which the docked, primed, and domain bound pools were combined into a single pool that we call the "primed" pool. We use this simplified model (Fig. 2), which is similar to a model of exocytosis in melanotroph cells (16) in all simulations. Here, the granule can be in one of four different states: a primed state where the granule is adjacent to the plasma membrane ($N_0$), or states in which one ($N_1$), two ($N_2$), or three ($N_3$) $Ca^{2+}$ ions are bound to the $Ca^{2+}$ sensor, likely synaptotagmin (31). Once in state $N_3$ the granule fuses with the membrane and releases its hormone content at rate $u_1$. Granule release is triggered by local $Ca^{2+}$ levels ($C_{loc}$), as indicated in Fig. 2, while resupply is dependent on the bulk calcium concentration $C_i$, which is computed as the submembrane $Ca^{2+}$ concentration 1.5 μm from the channel. The rate of resupply per cell $r_1$ is

$$r_1 = \frac{C_i(t) r_1^0}{C_i(t) + K_p}, \tag{8}$$

with $K_p$ =2.3 μM (4, 40), and $r_1^0$ is the maximal resupply rate per cell.

All secretion model steps are assumed to be reversible, except for fusion. The local $Ca^{2+}$ concentration was determined by solving the $Ca^{2+}$ reaction-diffusion equations and using the $Ca^{2+}$ value at the release site (Eqs. 6,7). The exocytosis model describing release per cell is given by the following differential equations:

$$\begin{aligned}
\frac{dN_0}{dt} &= -\left(3k_1 C_{loc}(t) + r_{-1}\right) N_0 + r_1(C_i(t)) + k_{-1} N_1, \\
\frac{dN_1}{dt} &= -\left(2k_1 C_{loc}(t) + k_{-1}\right) N_1 + 3k_1 C_{loc}(t) N_0 + 2k_{-1} N_2, \\
\frac{dN_2}{dt} &= -\left(k_1 C_{loc}(t) + 2k_{-1}\right) N_2 + 2k_1 C_{loc}(t) N_1 + 3k_{-1} N_3, \\
\frac{dN_3}{dt} &= -\left(u_1 + 3k_{-1}\right) N_3 + k_1 C_{loc}(t) N_2,
\end{aligned} \tag{9}$$

where $N_i$ is the number of granules in pool $i$. Experimental data (37) indicate a relatively low $Ca^{2+}$ binding affinity; as a consequence, we use the $Ca^{2+}$ affinity value $k_d = k_{-1}/k_1$=27 μM in Eqs. 9.

We used two sets of initial conditions for the granule/exocytosis model. In the model of Chen et al. (4) the number of primed granules (pool $N_0$) is equal to 40 per cell. Hence, we set as initial condition $N_0$=40 primed granules, each a fixed distance from a single channel (so 35 channels are not associated with granules). Assuming that – in any one simulation – all $Ca^{2+}$ channels in the cell behave identically according to the Markov simulation, the granules will be exposed to the same $Ca^{2+}$ profile. To calculate average cellular exocytosis, we performed 10 (single channel) or 5 (cluster) simulations and computed average values of $N_i$ at each time point.

This initial condition ($N_0$=40) reflects experiments such as single-cell capacitance measurements of triggered exocytosis, where no exocytosis is occurring before the experiment (36, 37). For

231 interpreting hormone secretion experiments, where secretion is ongoing, the steady state of the
232 model is more relevant. We found that the pools empty within seconds (see Results), and
233 therefore considered initial conditions where all pools are empty to reflect secretion experiments.

234 The exocytosis rate per cell, with $N_3$ the average of 10 or 5 trials as explained above, is

$$J_F(t) = u_1 N_3(t), \tag{10}$$

235 and the cumulative number of fused granules per cell is

$$M_F(t) = \int_0^t u_1 N_3(t')dt'. \tag{11}$$

236 To show how much of the simulated secretion is due to increased $Ca^{2+}$ influx during
237 bursting compared to spiking electrical activity, that is, to investigate whether bursting increases
238 the $Ca^{2+}$-current sensitivity of exocytosis (26), we related exocytosis to the total charge entering
239 via the $Ca^{2+}$ channel or channel cluster (26):

$$Q(t) = \int_0^t I_{sc} ds. \tag{12}$$

240 The exocytosis model was solved using the MATLAB (R2012b, The MathWorks®)
241 function ode15s.

242 [Figure 2]

243

## RESULTS

### *Secretion evoked by $Ca^{2+}$ influx through single channels is increased when converting spiking to bursting electrical activity through dynamic clamp*

Gonadotrophs release little LH under basal conditions, which has been suggested to be associated to their typical spiking electrical behavior (10). We have previously shown that adding a BK-type $K^+$ current to a spiking gonadotroph can change its behavior into bursting (35). Figure 3 shows an example of such a cell where the injected BK-type current induces bursting in an otherwise spiking gonadotroph. We also show the average of 10 independent simulations, each with a stochastic $Ca^{2+}$ channel providing $Ca^{2+}$ to the interior of the cell and subsequent $Ca^{2+}$ diffusion. The $Ca^{2+}$ model is driven by either the spiking voltage pattern (left) or the bursting pattern (right) obtained by injecting a BK-type $K^+$ current via dynamic clamp. Average $Ca^{2+}$ profiles are reported at distances of 30, 200, and 1500 nm from the $Ca^{2+}$ channel. As expected, close to the channel, i.e., 30 nm, $Ca^{2+}$ reaches high concentrations of some tens of micromolar on average with peaks up to ~70 μM during spiking activity and ~110 μM during bursting. The traces are very noisy due to the stochastic openings of the $Ca^{2+}$ channel. The average $Ca^{2+}$ concentration decreases with distance from the channel, reaching less than 1 μM at a distance of 1500 nm. In addition, the noise is attenuated due to the effects of diffusion, which acts as a low-pass filter. $Ca^{2+}$ measurements using a fluorescent dye such as fura-2 report on the $Ca^{2+}$ concentration averaged over the cell, and have time courses similar to those shown in the bottom row of Fig. 3 (30, 32).

[Figure 3]

We now locate the exocytosis machinery at different distances from the $Ca^{2+}$ channel and use the $Ca^{2+}$ concentration at that location to drive the exocytosis model (Fig. 2 and Eqs. 9). Figure 4 shows the average number of fused granules over time at different distances. If the release site is 30 nm from the channel, it is exposed to very high $Ca^{2+}$ concentrations, whether the cell is spiking or bursting, and exocytosis occurs at its maximum rate that releases all the granules in the primed pool $N_0$ (40 granules) very soon after the start of the input train. A similar

result occurs if the release site is located 100 nm from the channel. Thus, if the release site and channel are within 100 nm of each other it does not matter whether the cell is spiking or bursting, the secretion level will be the same, since the $Ca^{2+}$ concentrations at the exocytotic machinery are in both cases saturating. At a distance of 200 nm there is a difference between exocytosis evoked by spiking and that evoked by bursting; the bursting pattern (solid) evokes release at a higher rate than the spiking pattern (dashed), though both release almost all available granules by the end of the 5 second input train. The advantage of bursting over spiking is amplified when the release site is situated further from the channel, at 300 nm or 500 nm. Even though the absolute number of fused granules is lower when the channel and the release site are more distant, the bursting voltage trace releases more granules than the spiking trace at all time points. Thus, our simulations support the notion that adding an outward $K^+$ current can, by changing spiking to bursting activity, increase secretion (6, 29).

These observations imply that the primed pool of granules can be emptied very quickly, and this fusion process is likely monitored with capacitance measurements of exocytosis that take place over a short period of time (14). In our data, the spiking voltage trace shows 5 spikes in 5 seconds, each spike lasting ~40 ms (Fig. 3Ai). On average, each 40 ms depolarization of a pulse train was found to evoke ~10 fF of exocytosis (19). Thus, based on these experiments we expect ~50 fF exocytosis during the 5 seconds in Fig. 3. In our simulations, exocytosis at a distance of 200 nm from the channel is ~30 granules. If we assume that a single granule corresponds to ~2fF (39, 42), we get a capacitance measurement of ~60 fF, close to the ~50 fF calculated from (19).

[Figure 4]

However, most secretion measurements are made from a cell population over a period of minutes or tens of minutes. In such measurements the resupply of the primed pool by the reserve granule pool is rate limiting. We next look at the effects of resupply by emptying the primed pool $N_0$ at the beginning of the simulation and from this initial condition evaluate the differential exocytosis evoked by spiking and bursting.

The cumulative number of fused granules as a function of time is shown in Fig. 5 (top panel). Bursting evokes more release regardless of the distance between the channel and the

granule. This is in spite of the fact that at short distances the local $Ca^{2+}$ concentration saturates the release site, and highlights the importance of the dependence of resupply on the global, rather than local, $Ca^{2+}$ concentration. That is, the simulated global $Ca^{2+}$ concentration is higher during bursting than during spiking, as measured by fluorescent dyes (22), and this results in a greater rate of resupply in response to bursting. When the channel is close to the release site all granules becoming available due to the resupply are fused almost immediately, so resupply is rate limiting. Farther than 200 nm from the channel, local $Ca^{2+}$ concentrations start to play a predominant role since the exocytosis machinery is no longer saturated, and therefore differences in local $Ca^{2+}$ levels as well as global levels are responsible for differences in the exocytosis rates.

[Figure 5]

There are two factors that could contribute to the greater effectiveness of bursting at evoking secretion in the model. One is that bursting brings in more $Ca^{2+}$ over the 5 seconds of simulation time, increasing resupply rate relative to spiking, as mentioned above. The other is that the dynamics of $Ca^{2+}$ diffusion and the exocytotic machinery favor the bursting signal over the spiking signal. That is, bursting is more efficient than spiking at evoking release. To test the latter, we plot the number of fused granules versus the total $Ca^{2+}$ entry $Q$ (Fig. 5, bottom panels). For release sites closer than 200 nm from the channel the efficiencies of the spiking and bursting patterns are virtually the same. It is only at distances of 200 nm or greater that bursting becomes more efficient than spiking, since at these distances the number of fused granules per total $Ca^{2+}$ entry is larger when the cell is bursting. This is due to the longer duration of the bursting events, which produce longer-duration $Ca^{2+}$ signals that are advantageous for the exocytosis machinery that requires the binding of three $Ca^{2+}$ ions to evoke granule fusion. In fact, in simulations in which only two $Ca^{2+}$ ions are needed to evoke fusion the efficiencies of spiking and bursting are the same at a 200 nm distance, and bursting is only slightly more efficient at 300 and 500 nm distances (not shown).

As a final quantification of the effectiveness of bursting vs. spiking at evoking secretion we show the ratio between bursting-evoked secretion and spiking-evoked secretion in Fig. 6 (solid line). This ratio is calculated from the total number of fused granules at the end of the 5-sec input voltage train as a function of distance between the channel and the release site. Up until

a distance of 100 nm the ratio is ~1.5; the burst pattern evokes a slightly higher amount of secretion than spiking. Past this distance the ratio increases continuously, reaching a value of ~8.5 at a distance of 700 nm. Thus, there is between 1.5 and 8.5 times more secretion by the end of the 5-sec stimulation with bursting versus spiking. Plotting the ratio of exocytosis during spiking and bursting but normalized to the charge $Q$ (Fig. 6, dashed line) shows that spiking and bursting have almost the same $Ca^{2+}$ current sensitivity close to the channel (i.e., they are equally efficient at evoking release), but farther away bursting becomes more efficient than spiking, reaching a 5.5-fold higher $Ca^{2+}$ current sensitivity at a distance of 700 nm from the channel.

In summary, our simulations suggest that LH secretion from a gonadotroph could increase substantially if the electrical pattern switched from spiking to bursting, for example because of the addition of a BK-type current.

[Figure 6]

*Secretion evoked by $Ca^{2+}$ influx through a cluster of channels*

The previous simulations assumed that each release site is acted upon by $Ca^{2+}$ from single channels, and indeed there is evidence supporting this, in both endocrine cells and in neuronal synapses (11, 17). However, it is likely that hormone release sites receive $Ca^{2+}$ from several channels, and there is also evidence for this (2, 3). In the next set of simulations we consider such a situation, where a release site is affected by $Ca^{2+}$ from a cluster of 5 stochastic $Ca^{2+}$ channels. For simplicity we assume that these are equidistant from the release site.

Figure 7 shows the $Ca^{2+}$ concentration at different distances from the channel cluster in response to the spiking or bursting voltage trace. Close to the cluster (30 nm), $Ca^{2+}$ rises to a level of several hundreds of micromolar, about five times larger than in the single-channel case. At greater distances, the increase over the single-channel level is less, since now the different clusters are 6600 nm apart so that a release site located 1500 nm from a cluster is >5000 nm from the next nearest cluster. In contrast, with uniform distribution of the same number of channels (the single channel case), a release site located 1500 nm from one channel was located the same distance from a second channel, so it received an equal amount of $Ca^{2+}$ from both. Hence, whereas a cluster of 5 channels provides ~5 times higher $Ca^{2+}$ levels to granules located close to

the channels, a granule located 1500 nm from channels will be exposed to just ~5/2=2.5 times higher $Ca^{2+}$ concentrations in the case of channel clusters compared to the single-channel configuration.

[Figure 7]

Figure 8 (upper panels) shows that bursting is always superior to spiking in evoking exocytosis when channels are in clusters and the primed pool is initially empty. In contrast, the difference in $Ca^{2+}$ current sensitivity is hardly observable when the release site is less than 300 nm from the channel cluster (Fig. 8, lower panels). It is therefore mostly the larger amount of $Ca^{2+}$ entering during bursting that determines the difference in secretion. Figure 9 summarizes the results for channel clusters. Even at the closest release site/cluster distances the bursting-to-spiking ratio of the total number of fused granules is ~1.5, and increases to ~4.5 at 700 nm (solid line). The relative efficiency, i.e., the bursting-to-spiking ratio of the total number of granules normalized to $Ca^{2+}$ entry, is ~1 up to 300 nm, and increases then to ~2.5 at 700 nm. Thus, just as with single-channel-evoked release, bursting provides more secretion than does spiking when exocytosis is triggered by channel clusters. However, the advantage of bursting over spiking becomes manifest at greater distances for clusters than for single channels, 100 nm in Fig. 6 vs. 300 nm in Fig. 9.. Because the trends are qualitatively similar with single-channel and cluster-evoked secretion, we focus on only one type (single-channel secretion) in the remaining simulations.

[Figure 8]

[Figure 9]

*Bursting superiority depends on the frequency of spiking*

As a second example, we now use recordings from a GH4 cell line. It has previously been shown that pseudo-plateau bursting in some pituitary cells converts to spiking when BK-type $K^+$ channels are pharmacologically blocked, reducing the bulk $Ca^{2+}$ concentration (8). Does this manipulation also result in a decrease of the domain $Ca^{2+}$ and therefore in decreased secretion? We have shown that bursting can be rescued by adding BK current back to the cell using the dynamic clamp technique (here and in (34)). In Fig. 10 we use both procedures. We begin with a bursting lacto-somatroph GH4C1 cell (left column), then convert it to a spiking cell by the

addition of the BK channel blocker iberiotoxin (middle column), and finally convert the spiking cell back to a bursting cell using dynamic clamp to inject a model BK current (right column). For each case we calculate the $Ca^{2+}$ concentration at varying distances from the single stochastic channel, as in prior simulations. Close to the channel, the $Ca^{2+}$ concentration is about the same for all three voltage traces. However, at the greater distances, 1500 nm, the $Ca^{2+}$ levels corresponding to the bursting voltage traces are higher than those corresponding to the spiking voltage trace, as has been observed in experiments (18).

We next use these $Ca^{2+}$ time courses to simulate exocytosis for release sites located at different distances from the $Ca^{2+}$ channel (Fig. 11). The results are summarized in Fig. 12, where we show the number of fused granules evoked by the dynamic clamp-induced bursting vs. that evoked by the spiking trace (solid black curve). In both cases, the ratio is near 1 up until a separation distance of ~150-200 nm. At greater separations the ratio increases, indicating that at these greater distances the bursting trace is more effective at evoking exocytosis than the spiking trace. Normalizing to $Ca^{2+}$ influx reveals that the ratio of $Ca^{2+}$ current sensitivity is higher for spiking close to the channel (ratio $< 1$) whereas bursting is more efficient farther from the channel (Fig. 12). The fact that bursting is less superior to spiking after normalizing to $Ca^{2+}$ influx compared to the previous simulations of exocytosis using the traces from a gonadotroph (Figs. 5 and 6) can be explained by noticing that, for this example, iberiotoxin-induced spiking (Fig. 10B) occurs at a much higher rate (~1.8 Hz) than bursting (~0.8 Hz) (Fig 10A, C). Thus, the dynamics of $Ca^{2+}$ entry is important for the control of exocytosis in addition to the number of $Ca^{2+}$ ions entering the cell.

[Figure 10]

[Figure 11]

[Figure 12]

## DISCUSSION

In the absence of hypothalamic stimulation or inhibition, pituitary lactotrophs and somatotrophs release prolactin and growth hormone, while gonadotrophs comparatively secrete a negligible amount of luteinizing hormone. This difference in basal hormone release was matched by differences in spontaneous electrical activity between these cell types: lactotrophs and somatotrophs often exhibit "pseudo-plateau" bursts of activity, causing periodic $Ca^{2+}$ influx, while gonadotrophs usually produce spikes that are too brief to perturb the bulk $Ca^{2+}$ level substantially (9). Such differences in the bulk $Ca^{2+}$ profiles lead to the hypothesis that different patterns of spontaneous electrical activity result in different rates of hormone release. Bursting causes hormone release from lactotrophs and somatotrophs, while spiking causes no hormone release from gonadotrophs.

We tested this hypothesis in this paper. While $Ca^{2+}$ triggers hormone release and bursting creates larger amplitude oscillations of average intracellular $Ca^{2+}$ than spiking, this does not necessarily mean that bursting is more effective at triggering hormone release. The $Ca^{2+}$ concentration that matters is that seen by the hormone-containing granules at their release sites, and if the release sites are close to $Ca^{2+}$ channels, the high $Ca^{2+}$ concentration in the microdomains around the channels created by a single spike may be just as effective as that due to a burst in triggering fusion of granules. Indeed, we found that spiking is as effective as bursting in releasing a full pool of primed granules, as long as the release site is within 100 nm from the channel (Fig. 4). However, if the primed pool of granules is initially empty, or if the release site is located more than 100 nm from the channel, we found that bursting was always more effective than spiking in triggering granule fusion.

There are two mechanisms for this difference between bursting and spiking. The first results from the larger entry of $Ca^{2+}$ caused by bursting over spiking. Because the fraction of open $Ca^{2+}$ channels is increased for a longer period of time during a burst than during a spike, a burst causes a larger increase in bulk $Ca^{2+}$. Since the replenishment of the primed pool of granules depends on bulk $Ca^{2+}$, bursting causes a higher rate of granules priming, which in turn results in a higher rate of granule fusion. This effect is independent of the microdomain $Ca^{2+}$ concentration, so bursting causes a higher rate of granule fusions even if the release site is 100 nm or less from the channel (Fig. 5 top panels). However, this mechanism relies on the fact that,

441 at similar event frequency, bursting means that the electric potential across the cell membrane
442 stays high (i.e., at levels where the cell $Ca^{2+}$ current is high) for a larger fraction of time than
443 spiking. If spiking frequency is increased relative to bursting frequency so that the total amount
444 of active time is the same, then bulk $Ca^{2+}$ will be similar and so will the priming rate. In that
445 sense, the bursting pattern is not more effective than the spiking pattern if the amount of activity
446 (and therefore $Ca^{2+}$ entry) is normalized.

447 Nevertheless, there is a second mechanism that makes bursting more effective than
448 spiking at triggering granule fusion, even if we normalize by the total amount of $Ca^{2+}$ entry.
449 Because three free $Ca^{2+}$ ions must bind to the release machinery to trigger fusion, fusion is
450 facilitated by a stable high local $Ca^{2+}$ level. This is more likely to happen during bursting than
451 spiking, since $Ca^{2+}$ influx can be maintained longer during a burst than during a spike. This
452 advantage of bursting can be observed when the release site is more than 100 nm away from the
453 channel (Fig. 5 bottom panels). Cells must quickly restore intracellular $Ca^{2+}$ to low levels using
454 ATP-driven pumps, so there is an energetic cost associated with the entry of each $Ca^{2+}$ ion. For
455 release sites far from the $Ca^{2+}$ channels, the bursting pattern of activity results in a more efficient
456 use of $Ca^{2+}$ ions than the spiking pattern.

457 This may not be true at higher spike frequencies. If we increase spike frequency the
458 interval between each increase in local $Ca^{2+}$ goes down, so the higher effectiveness of bursting
459 might only be observed for release sites further away from the channels. We see that for the BK
460 (endogenous or injected by dynamic clamp) vs. no BK (i.e., in the presense of iberiotoxin) case,
461 where the maximum $Ca^{2+}$ concentration reached at 200 nm (Fig. 10) is similar to what we saw in
462 Fig. 3, but the interspike interval is lower so $Ca^{2+}$ does not go back down for long – in that case
463 spiking is at least as efficient as bursting in evoking release, for release sites up to 500 nm away
464 from the channels (Fig. 11). Nevertheless, the bursting pattern caused by the presence of a BK
465 current evoked more granule fusion because of the high average bulk $Ca^{2+}$ during bursting,
466 which results in higher rate of replenishment of the primed granules.

467 There are many examples in endocrinology where the pattern of a signal plays an
468 important role. A well-known example is that the frequency of hypothalamic gonadotropin-
469 releasing hormone pulses determines the differential release of luteinizing and follicle-

stimulating hormone by gonadotrophs (41). Here we used a hybrid experimental/modeling approach to show that the actual pattern of electrical activity can trigger different rates of hormone release. Since the discovery that pituitary cells are electrically active 40 years ago, researchers have wondered how pituitary cells tune electrical activity to regulate hormone release (24). It has been argued that since hypothalamic factors act on a number of ion channels on pituitary cell membranes, electrical activity provides numerous ways for the hypothalamus to modulate pituitary hormone release. Some of these factors may even modulate the time constant of BK channels to switch the electrical activity pattern from spiking to bursting (6). The present work shows that this switch to bursting may improve the effect of hypothalamic stimulating neurohormones in increasing pituitary hormone secretion.

In summary, our modeling results show that bursting is superior to spiking in evoking pituitary hormone release, since it brings more $Ca^{2+}$ into the cell, thus augmenting both local and global $Ca^{2+}$ levels, which in turn increases resupply of secretory granules and exocytosis. We found further that channel clustering is advantageous to isolated channels in controlling secretion. Our results have implications beyond pituitary secretion. For example, human pancreatic beta-cells show rapid bursting resembling pituitary plateau bursting (23, 27), which has been suggested to be advantageous for insulin secretion (25). Further, $Ca^{2+}$ channel clustering in beta-cells has been suggested to be important for insulin exocytosis (2).

## GRANTS

JT and RB were partially supported by grant DMS1220063 from the National Science Foundation.

## DISCLOSURES

No conflicts of interest, financial or otherwise, are declared by the authors.

## REFERENCES


1. **Allbritton NL, Meyer T, Stryer L**. Range of messenger action of calcium ion and inositol 1,4,5-trisphosphate. *Science* 258: 1812–5, 1992.

2. **Barg S, Ma X, Eliasson L, Galvanovskis J, Göpel SO, Obermüller S, Platzer J, Renström E, Trus M, Atlas D, Striessnig J, Rorsman P**. Fast exocytosis with few Ca(2+) channels in insulin-secreting mouse pancreatic B cells. *Biophys. J.* 81: 3308–23, 2001.

3. **Bertram R, Smith GD, Sherman A**. Modeling study of the effects of overlapping Ca2+ microdomains on neurotransmitter release. *Biophys. J.* 76: 735–50, 1999.

4. **Chen Y, Wang S, Sherman A**. Identifying the targets of the amplifying pathway for insulin secretion in pancreatic beta-cells by kinetic modeling of granule exocytosis. *Biophys. J.* 95: 2226–2241, 2008.

5. **Dubinsky JM, Oxford GS**. Ionic currents in two strains of rat anterior pituitary tumor cells. *J. Gen. Physiol.* 83: 309–339, 1984.

6. **Duncan PJ, Sengul S, Tabak J, Ruth P, Bertram R, Shipston MJ**. Large conductance Ca(2+) -activated K(+) channels (BK) promote secretagogue-induced transition from spiking to bursting in murine anterior pituitary corticotrophs. *J. Physiol.* 593: 1197–1211, 2015.

7. **Freeman ME, Kanyicska B, Lerant A, Gyorgy N**. Prolactin: Structure , Function , and Regulation of Secretion. *Physiol. Rev.* 80: 1523–1631, 2000.

8. **Van Goor F, Li Y-X, Stojilkovic SS**. Paradoxical Role of Large-Conductance Calcium-Activated K+ (BK) Channels in Controlling Action Potential-Driven Ca2+ Entry in Anterior Pituitary Cells. *J. Neurosci.* 21: 5902–5915, 2001.

9. **Van Goor F, Zivadinovic D, Martinez-Fuentes AJ, Stojilkovic SS**. Dependence of pituitary hormone secretion on the pattern of spontaneus voltage-gated calcium influx. Cell type-specific action potential secretion coupling. *J. Biol. Chem.* 276: 33840–33846, 2001.

10. **Van Goor F, Zivadinovic D, Stojilkovic SS**. Differential expression of ionic channels in rat anterior pituitary cells. *Mol. Endocrinol.* 15: 1222–1236, 2001.

11. **Hagiwara S, Ohmori H**. Studies of single calcium channel currents in rat clonal pituitary cells. *J. Physiol.* 336: 649–61, 1983.

12. **Hodgking AL, Huxley AF**. A quantitative description of membrane current and its application to conduction and excitation in nerve. *J. Physiol.* 117: 500–44, 1952.

13. **Keja JA, Kits KS**. Single-channel properties of high- and low-voltage-activated calcium channels in rat pituitary melanotropic cells. *J. Neurophysiol.* 71: 840–55, 1994.

14. **Kits KS, Mansvelder HD**. Regulation of exocytosis in neuroendocrine cells: Spatial organization of channels and vesicles, stimulus-secretion coupling, calcium buffers and modulation. *Brain Res. Rev.* 33: 78–94, 2000.

15. **Kits KS, de Vlieger T a, Kooi BW, Mansvelder HD**. Diffusion barriers limit the effect of mobile calcium buffers on exocytosis of large dense cored vesicles. *Biophys. J.* 76: 1693–1705, 1999.

16. **Kits KS, de Vlieger T a, Kooi BW, Mansvelder HD**. Diffusion barriers limit the effect of mobile calcium buffers on exocytosis of large dense cored vesicles. *Biophys. J.* 76: 1693–1705, 1999.

17. **Klingauf J, Neher E**. Modeling buffered Ca2+ diffusion near the membrane: implications for secretion in neuroendocrine cells. *Biophys. J.* 72: 674–90, 1997.

18. **Li YX, Rinzel J, Vergara L, Stojilković SS**. Spontaneous electrical and calcium oscillations in unstimulated pituitary gonadotrophs. *Biophys. J.* 69: 785–95, 1995.

19. **Mansvelder HD, Kits KS**. The relation of exocytosis and rapid endocytosis to calcium entry evoked by short repetitive depolarizing pulses in rat melanotropic cells. *J. Neurosci.* 18: 81–92, 1998.

20. **Matveev V, Zucker RS, Sherman A**. Facilitation through buffer saturation: constraints on endogenous buffering properties. *Biophys. J.* 86: 2691–2709, 2004.

21. **Matveev V**. CalC • The Calcium Calculator • Victor Matveev, NJIT. https://web.njit.edu/~matveev/.

22. **Milescu LS, Yamanishi T, Ptak K, Mogri MZ, Smith JC**. Real-time kinetic modeling of voltage-gated ion channels using dynamic clamp. *Biophys. J.* 95: 66–87, 2008.

23. **Misler S, Barnett DW, Gillis KD, Pressel DM**. Electrophysiology of stimulus-secretion coupling in human beta-cells. *Diabetes* 41: 1221–8, 1992.

24. **Mollard P, Schlegel W**. Why are endocrine pituitary cells excitable? *Trends Endocrinol. Metab.* 7: 361–365, 1996.

25. **Pedersen MG, Cortese G, Eliasson L**. Mathematical modeling and statistical analysis of calcium-regulated insulin granule exocytosis in beta-cells from mice and humans. *Prog. Biophys. Mol. Biol.* 107: 257–264, 2011.

26. **Pedersen MG**. On depolarization-evoked exocytosis as a function of calcium entry: Possibilities and pitfalls. *Biophys. J.* 101: 793–802, 2011.

27. **Riz M, Braun M, Pedersen MG**. Mathematical modeling of heterogeneous electrophysiological responses in human β-cells. *PLoS Comput. Biol.* 10: e1003389, 2014.

28. **Sherman A, Keizer J, Rinzel J**. Domain model for Ca2(+)-inactivation of Ca2+ channels at low channel density. *Biophys. J.* 58: 985–95, 1990.

29. **Stojilkovic SS, Tabak J, Bertram R**. Ion channels and signaling in the pituitary gland. *Endocr. Rev.* 31: 845–915, 2010.

30. **Stojilkovic SS, Zemkova H, Van Goor F**. Biophysical basis of pituitary cell type-specific Ca2+ signaling-secretion coupling. *Trends Endocrinol. Metab.* 16: 152–9, 2005.

31. **Stojilkovic SS**. Ca2+-regulated exocytosis and SNARE function. *Trends Endocrinol. Metab.* 16: 81–83, 2005.

32. **Stojilkovic SS**. Pituitary cell type-specific electrical activity, calcium signaling and secretion. *Biol. Res.* 39: 403–423, 2006.

33. **Tabak J, Gonzalez-Iglesias AE, Toporikova N, Bertram R, Freeman ME**. Variations in the response of pituitary lactotrophs to oxytocin during the rat estrous cycle. *Endocrinology* 151: 1806–13, 2010.

34. **Tabak J, Tomaiuolo M, Gonzalez-Iglesias a. E, Milescu LS, Bertram R**. Fast-Activating Voltage- and Calcium-Dependent Potassium (BK) Conductance Promotes Bursting in Pituitary Cells: A Dynamic Clamp Study. *J. Neurosci.* 31: 16855–16863, 2011.

35. **Tashjian AH, Yasumura Y, Levine L, Sato GH, Parker ML**. Establishment of clonal strains of rat pituitary tumor cells that secrete growth hormone. *Endocrinology* 82: 342–52, 1968.

36. **Thomas P, Surprenant a, Almers W**. Cytosolic Ca2+, exocytosis, and endocytosis in single melanotrophs of the rat pituitary. *Neuron* 5: 723–733, 1990.

37. **Thomas P, Wong JG, Lee a K, Almers W**. A low affinity Ca2+ receptor controls the final steps in peptide secretion from pituitary melanotrophs. *Neuron* 11: 93–104, 1993.

38. **Tse A, Hille B**. GnRH-induced Ca2+ oscillations and rhythmic hyperpolarizations of pituitary gonadotropes. *Science.* 255: 462–464, 1992.

39. **Vardjan N, Jorgačevski J, Stenovec M, Kreft M, Zorec R**. Compound exocytosis in pituitary cells. *Ann. N. Y. Acad. Sci.* 1152: 63–75, 2009.

40. **Voets T**. Dissection of Three Ca2+-Dependent Steps Leading to Secretion in Chromaffin Cells from Mouse Adrenal Slices. *Neuron* 28: 537–545, 2000.

41. **Wildt L, Häusler A, Marshall G, Hutchison JS, Plant TM, Belchetz PE, Knobil E**. Frequency and amplitude of gonadotropin-releasing hormone stimulation and gonadotropin secretion in the rhesus monkey. *Endocrinology* 109: 376–85, 1981.

42. **Zorec R, Sikdar SK, Mason WT**. Increased cytosolic calcium stimulates exocytosis in bovine lactotrophs. Direct evidence from changes in membrane capacitance. *J. Gen. Physiol.* 97: 473–497, 1991.

FIGURE CAPTIONS

Figure 1. Calcium diffusion characteristics in the model. a) Spherical cell model used in simulations. The cell diameter is 13 μm. $Ca^{2+}$ diffusion and buffering are simulated in a conical region of the sphere. The channel or channel cluster is located at the center of the cone base on the surface of the sphere. The base radius in the single channel case is 1.5 μm and in the cluster case 3.3 μm. b) Upper panel: submembrane $Ca^{2+}$ concentrations (color coded, in μM) as a function of time and the distance to the channel (d, measured along the cone base as indicated in panel a) during spiking electrical activity. Lower panel: $Ca^{2+}$ concentration at 500 nm from the channel as function of time.

Figure 2. Kinetic scheme of the exocytosis model. The pool $N_0$ consists of granules primed for fusion and its resupply depends on the bulk cytosolic $Ca^{2+}$ concentration $C_i$. Fusion occurs upon $Ca^{2+}$ binding controlled by the local concentration of $Ca^{2+}$, $C_{loc}$. The pools $N_1$, $N_2$, $N_3$ correspond to the three $Ca^{2+}$ bound states, and $u_1$ is the fusion rate.

Figure 3. $Ca^{2+}$ concentration at different distances from a single stochastic $Ca^{2+}$ channel on the surface of a conical region (average of 10 independent trials). The $Ca^{2+}$ channel is placed at the center of the cone base with radius 1.5 μm. The $Ca^{2+}$ concentration is determined using a mathematical model, in response to actual spiking (A) and bursting (B) voltage traces from a gonadotroph. The switch to bursting was obtained by injecting a model BK-current into a spiking cell using the dynamic clamp technique.

Figure 4. Single channel exocytosis simulation results with $N_0$=40 primed granules as initial condition. Number of fused granules (average of 10 simulations) during spiking (dashed curve) and bursting (solid curve) electrical activity for different distances between the single $Ca^{2+}$ channel and a release site as a function of time.

Figure 5. Single channel exocytosis simulation results with all the pools initially empty. Top panels (i) show the number of fused granules as a function of time, as in Fig. 4. Bottom panels (ii) show the cumulative number of fused granules during 5 seconds of simulation as function of the cumulative calcium entry $Q$. (A) granules located at 30 nm, (B) 100 nm, (C) 200 nm, (D) 300 nm, or (E) 500 nm from the channel.

Figure 6. Summary of single channel exocytosis results with all the pools initially empty. The bursting-to-spiking ratio of the total number of fused granules during 5 seconds of electrical activity (solid line) shows that bursting evokes more secretion at all distances. In contrast, the bursting-to-spiking ratio of the total number of granules normalized to change entry $Q$ (dashed line) shows that the efficiency of spiking and bursting are comparable for release sites located close to the channel, but that bursting has superior efficiency farther from the channel.

Figure 7. $Ca^{2+}$ concentrations for a cluster of 5 channels (average of 5 independent trials). The $Ca^{2+}$ channel is placed at the center of the cone base with radius 3.3 μm. The $Ca^{2+}$ concentration is determined using the mathematical model, in response to actual spiking (A) and dynamic-clamp induced bursting (B) voltage traces from a gonadotroph (same traces as in Fig. 3).

Figure 8. Channel cluster exocytosis simulation results with all the pools initially empty. Top panels (i) show the number of fused granules as a function of time, evoked by spiking (dashed curve) or bursting (solid curve). Bottom panels (ii) show the cumulative number of fused granules during 5 seconds of simulation as a function of the cumulative $Ca^{2+}$ entry $Q$. (A) granules located at 30 nm, (B) 100 nm, (C) 200 nm, (D) 300 nm, or (E) 500 nm from the channel.

Figure 9. Summary of channel cluster exocytosis results with all the pools initially empty. The bursting-to-spiking ratio of the total number of fused granules during 5 seconds of electrical activity (solid line) shows that bursting evokes more secretion at all distances. In contrast, the bursting-to-spiking ratio of the total number of granules normalized to change entry $Q$ (dashed line) shows that the efficiency of spiking and bursting are comparable for release sites located close to the channel cluster, but that bursting has superior efficiency farther away.

Figure 10. $Ca^{2+}$ concentration at different distances from a stochastic $Ca^{2+}$ channel on the surface of a conical region (average of 10 independent trials). The $Ca^{2+}$ channel is placed at the center of the cone base with radius 1.5 μm. (A) Bursting profile in control condition. (B) Spiking profile in the presence of the BK channel blocker iberiotoxin. (C) Bursting profile in the presence of iberiotoxin and when BK current is injected back using the dynamic clamp. Sub panels show the experimentally recorded voltage profile (i), and simulated $Ca^{2+}$ concentrations at 30 nm (ii), 200 nm (iii), or 1500 nm (iv) from the channel.

660 Figure 11. Single channel exocytosis simulation results with all the pools initially empty for
661 dynamic clamp-induced bursting. Top panels (i) show the number of fused granules as a function
662 of time, evoked by a spiking voltage trace (gray dashed curves) and bursting induced by dynamic
663 clamp in the presence of iberiotoxin (black solid curves). Bottom panels (ii) show the
664 cumulative number of fused granules during 5 seconds of simulation as a function of the
665 cumulative $Ca^{2+}$ entry $Q$. (A) granules located at 30 nm, (B) 100 nm, (C) 200 nm, (D) 300 nm, or
666 (E) 500 nm from the channel.

667 Figure 12. Summary of exocytosis simulation results with all the pools initially empty during
668 BK-current block and dynamic clamp. The ratios of the total number of fused granules between
669 bursting that results from dynamic clamp application with iberiotoxin vs. spiking that results
670 from iberiotoxin alone (solid black curve). The ratios of the total number of fused granules
671 normalized to the charge entry $Q$ are given by the dashed curves.

672

673 Table 1. Default parameters of the $Ca^{2+}$ channel model, $Ca^{2+}$ diffusion simulations and
674 exocytosis model.

| Parameter | Value | Unit |
|---|---|---|
| **Current Simulation** | | |
| $s_m$ | 7 | mV |
| $v_m$ | -4 | mV |
| $k_+$ | 0.0234 | $ms^{-1}$ |
| $k_-$ | 0.018 | $ms^{-1}$ |
| $g_{Ca}$ | 20 | pS |
| **Diffusion Simulation** | | |
| $D_{Ca}$ | 0.22 | $\mu m^2 s^{-1}$ |
| $B_{total}$ | 900 | µM |
| $K_D$ | 10 | µM |
| $k_{on}$ | 0.1 | $\mu M^{-1} ms^{-1}$ |
| $k_{off}$ | 1 | $ms^{-1}$ |
| $[Ca^{2+}]_0$ | 0.22 | µM |
| **Secretion Model** | | |
| $k_1$ | 3.7 | $\mu M^{-1} s^{-1}$ |
| $k_{-1}$ | 100 | $s^{-1}$ |
| $r_1^0$ | 3.6 | $s^{-1}$ |
| $K_p$ | 2.3 | µM |
| $r_{-1}$ | 0.001 | $s^{-1}$ |
| $u_1$ | 1000 | $s^{-1}$ |

675

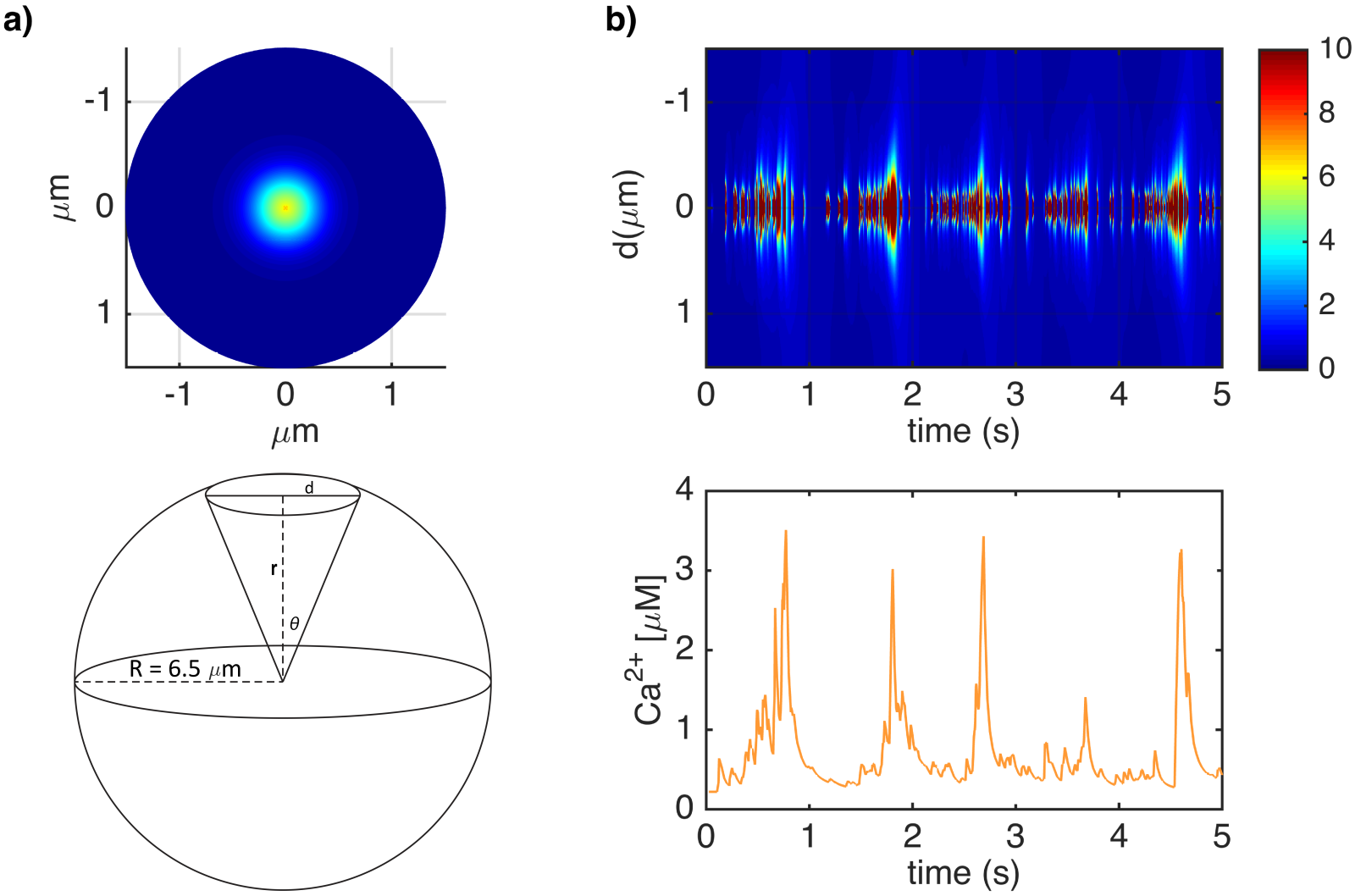
a)
b)
-1
0
1
μm
-1
0
1
μm
d
r
θ
R = 6.5 μm
d(μm)
-1
0
1
0
1
2
3
4
5
time (s)
10
8
6
4
2
0
Ca2+ [μM]
0
1
2
3
4
0
1
2
3
4
5
time (s)

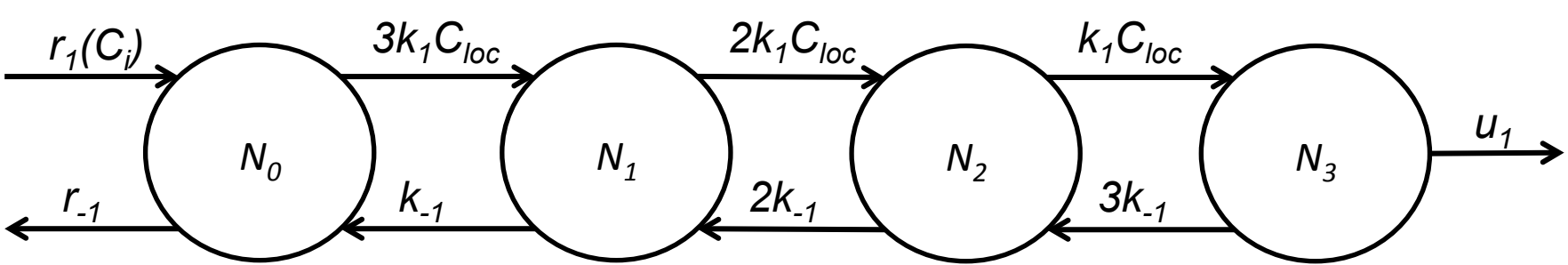
$r_1(C_i)$
$3k_1C_{loc}$
$2k_1C_{loc}$
$k_1C_{loc}$
$u_1$
$N_0$
$N_1$
$N_2$
$N_3$
$r_{-1}$
$k_{-1}$
$2k_{-1}$
$3k_{-1}$

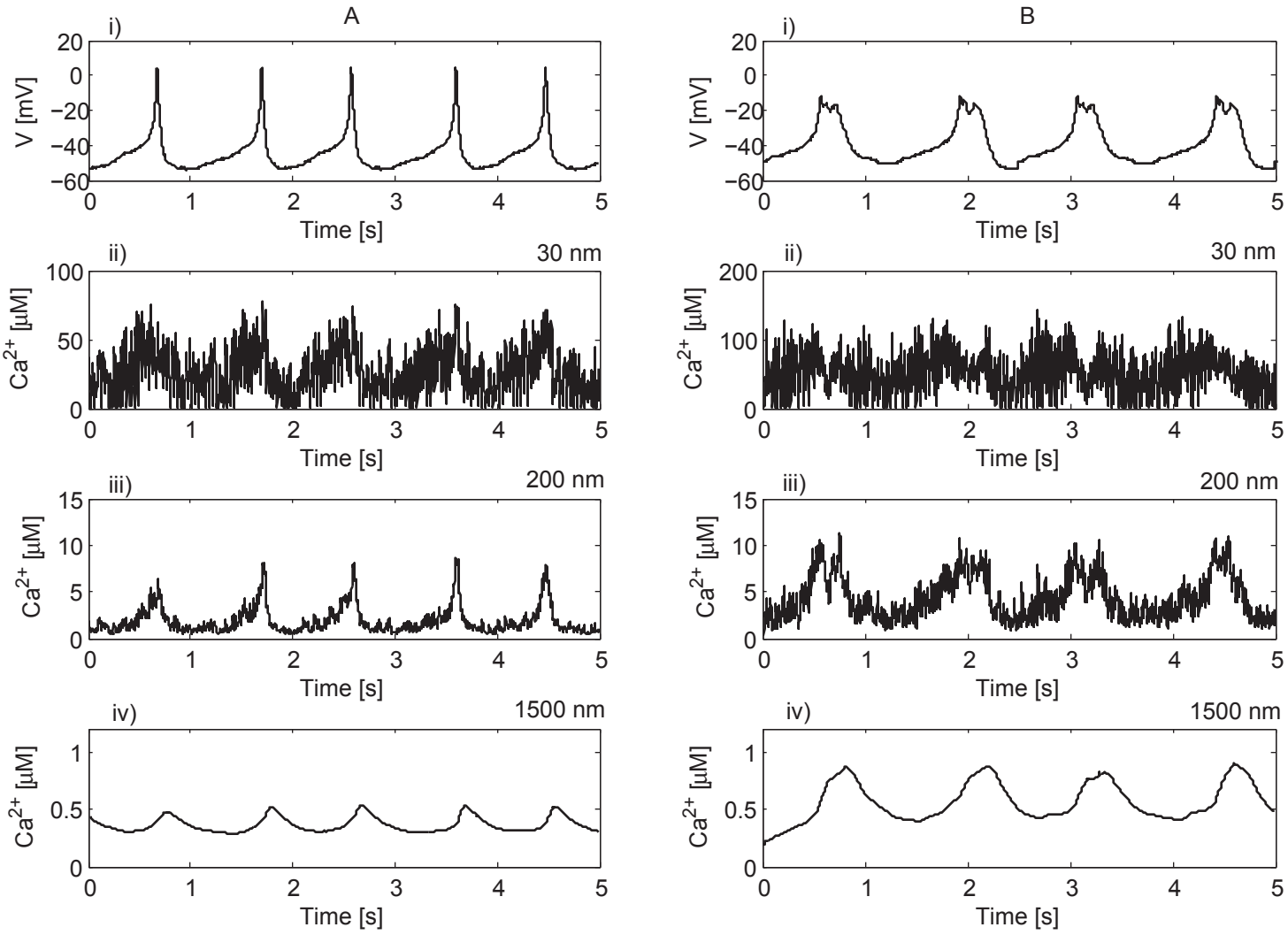
A
B
i)
ii)
iii)
iv)
30 nm
200 nm
1500 nm
V [mV]
Ca2+ [µM]
Time [s]

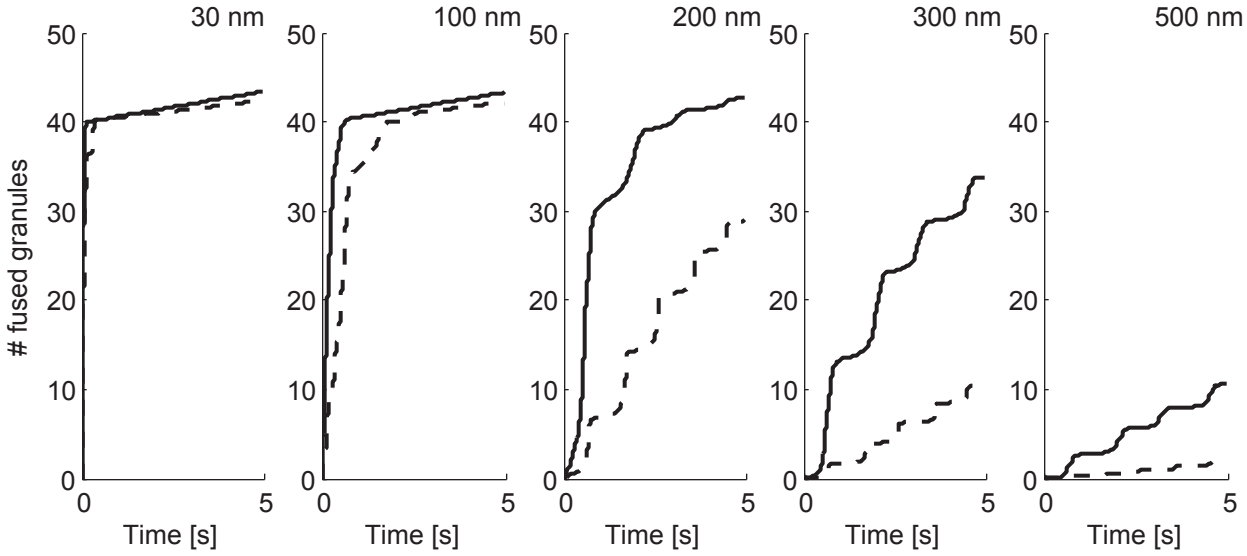
30 nm
100 nm
200 nm
300 nm
500 nm
# fused granules
Time [s]
0
10
20
30
40
50
5

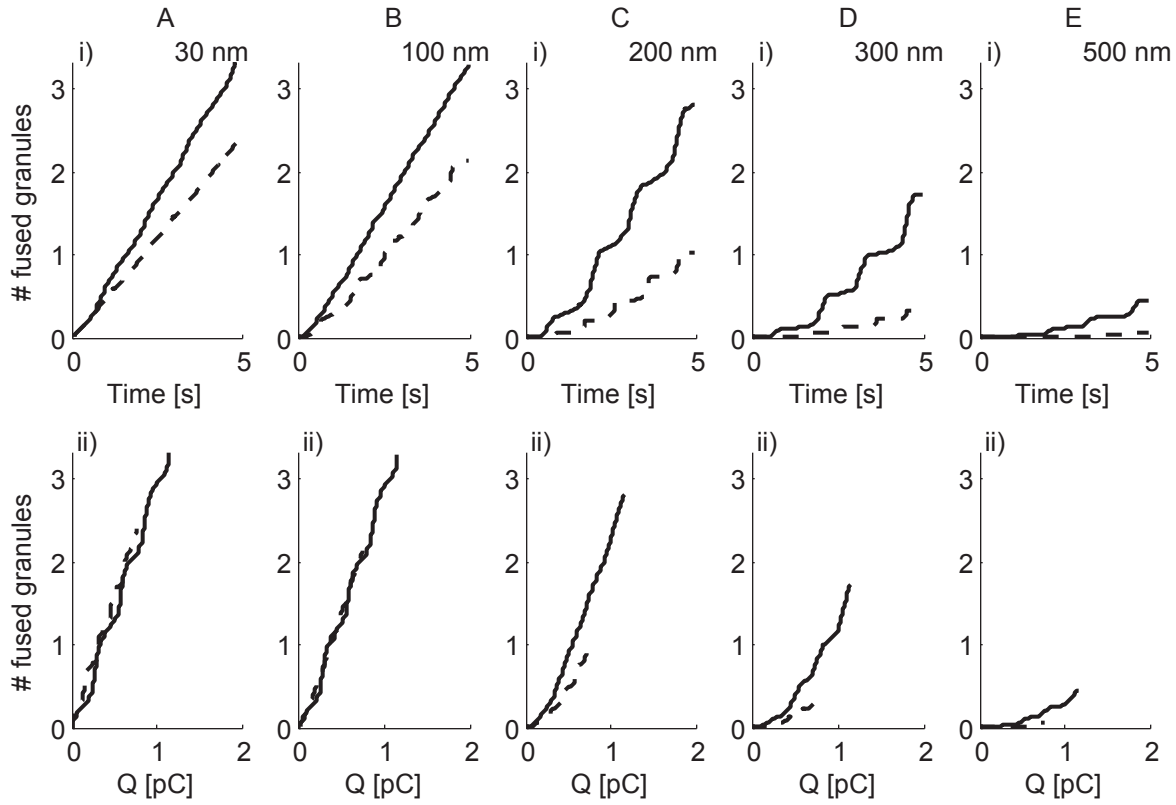
A
B
C
D
E
i)
30 nm
100 nm
200 nm
300 nm
500 nm
# fused granules
Time [s]
ii)
Q [pC]

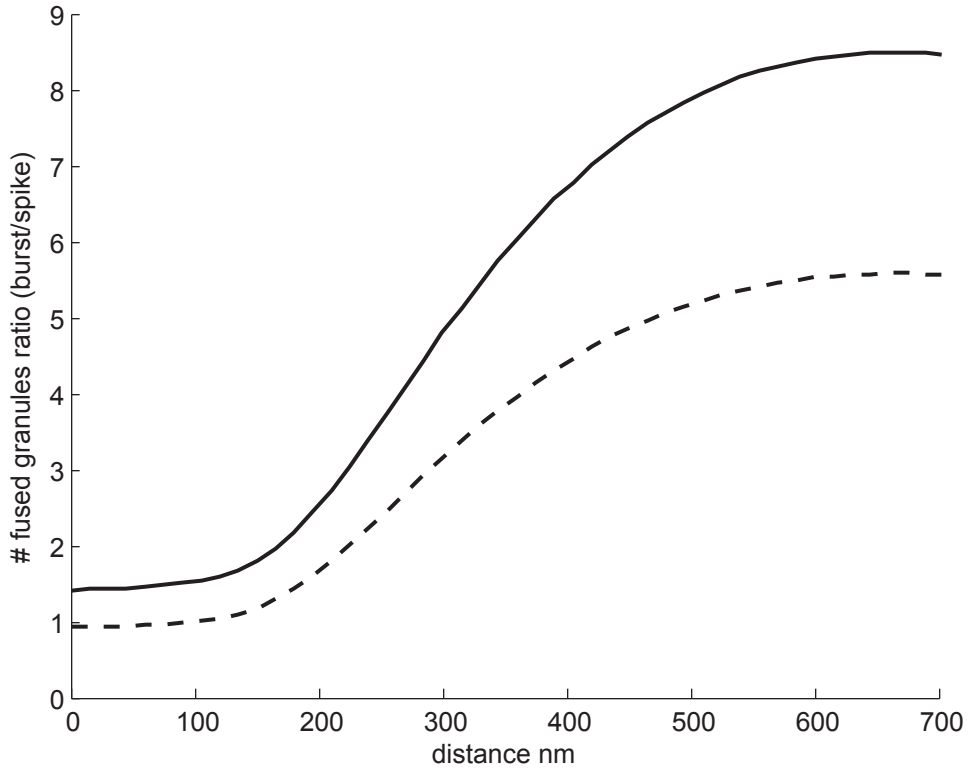
9
8
7
6
5
4
3
2
1
0
# fused granules ratio (burst/spike)
0
100
200
300
400
500
600
700
distance nm

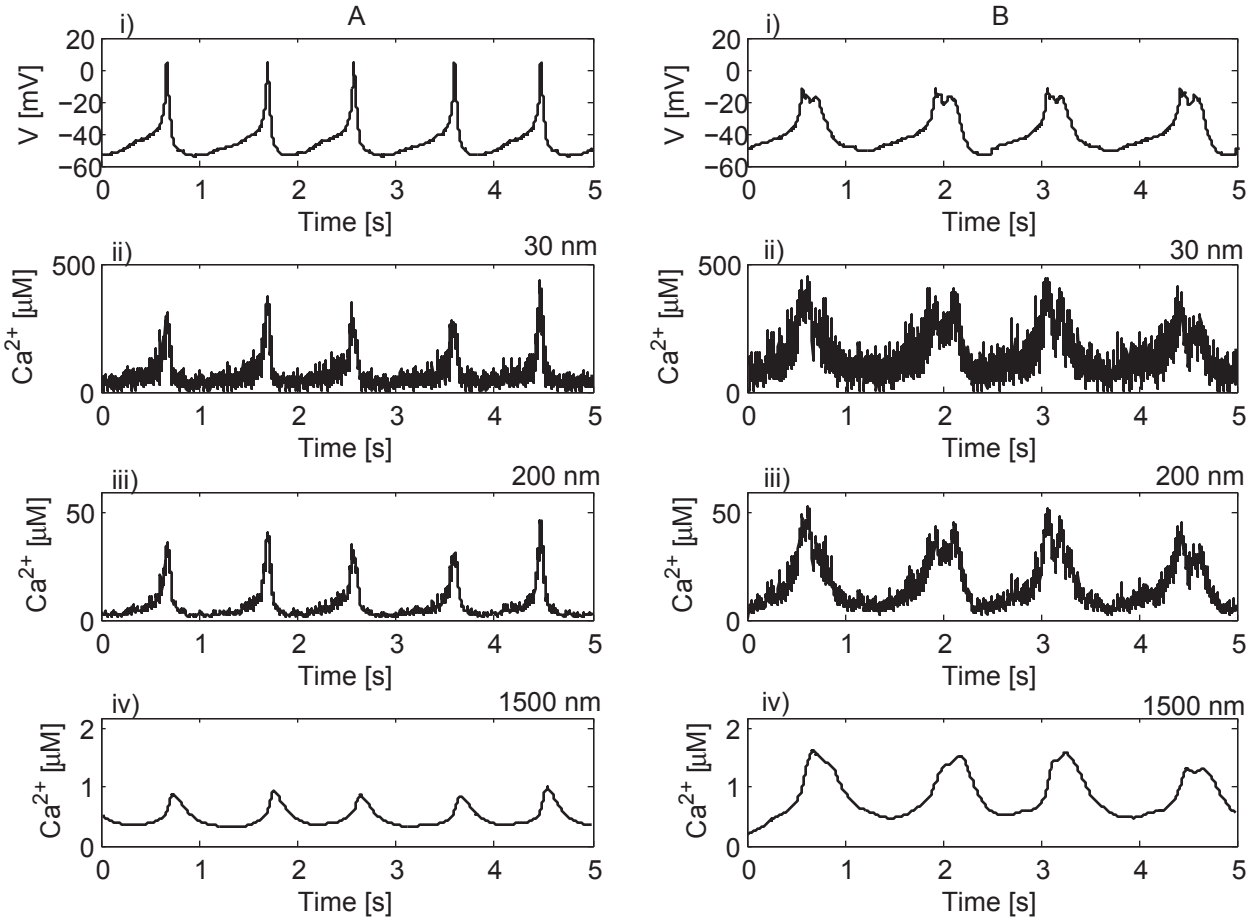
A
B
i)
ii)
iii)
iv)
30 nm
200 nm
1500 nm
V [mV]
Ca2+ [µM]
Time [s]

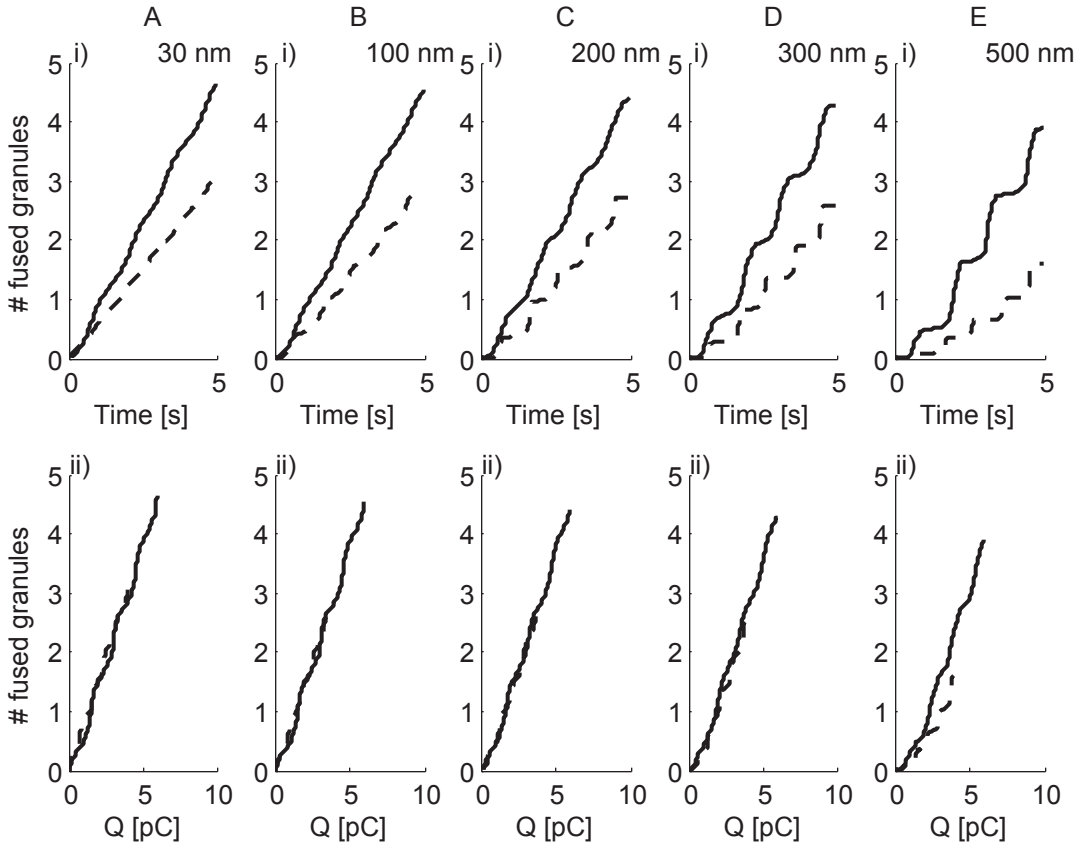
A
B
C
D
E
i)
30 nm
100 nm
200 nm
300 nm
500 nm
# fused granules
Time [s]
ii)
Q [pC]

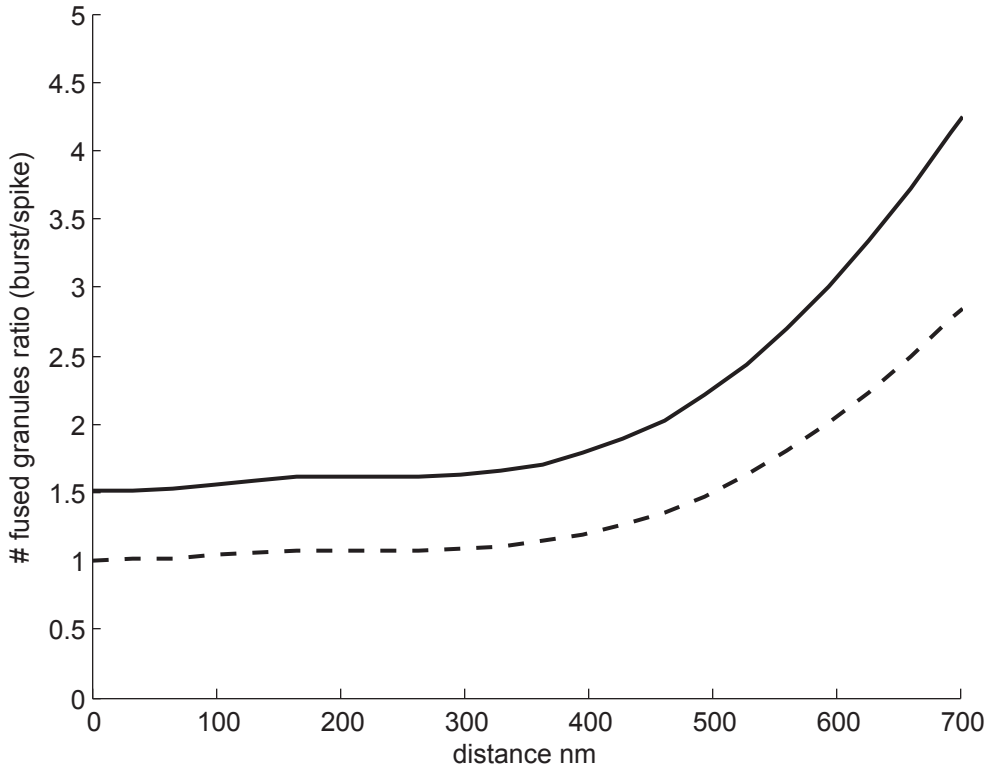
5
4.5
4
3.5
3
2.5
2
1.5
1
0.5
0
# fused granules ratio (burst/spike)
0
100
200
300
400
500
600
700
distance nm

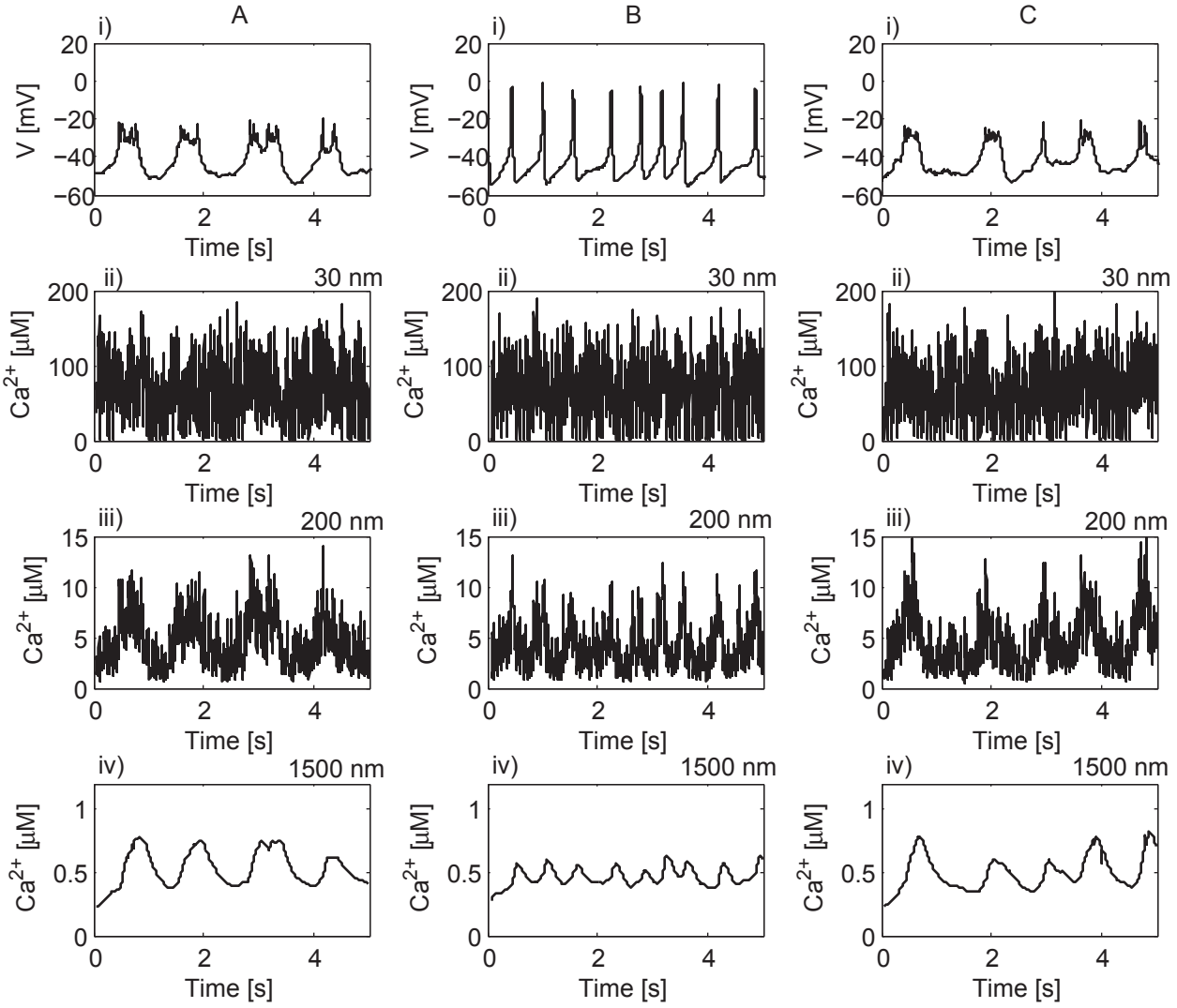
A
B
C
i)
ii)
iii)
iv)
30 nm
200 nm
1500 nm
V [mV]
Ca2+ [µM]
Time [s]

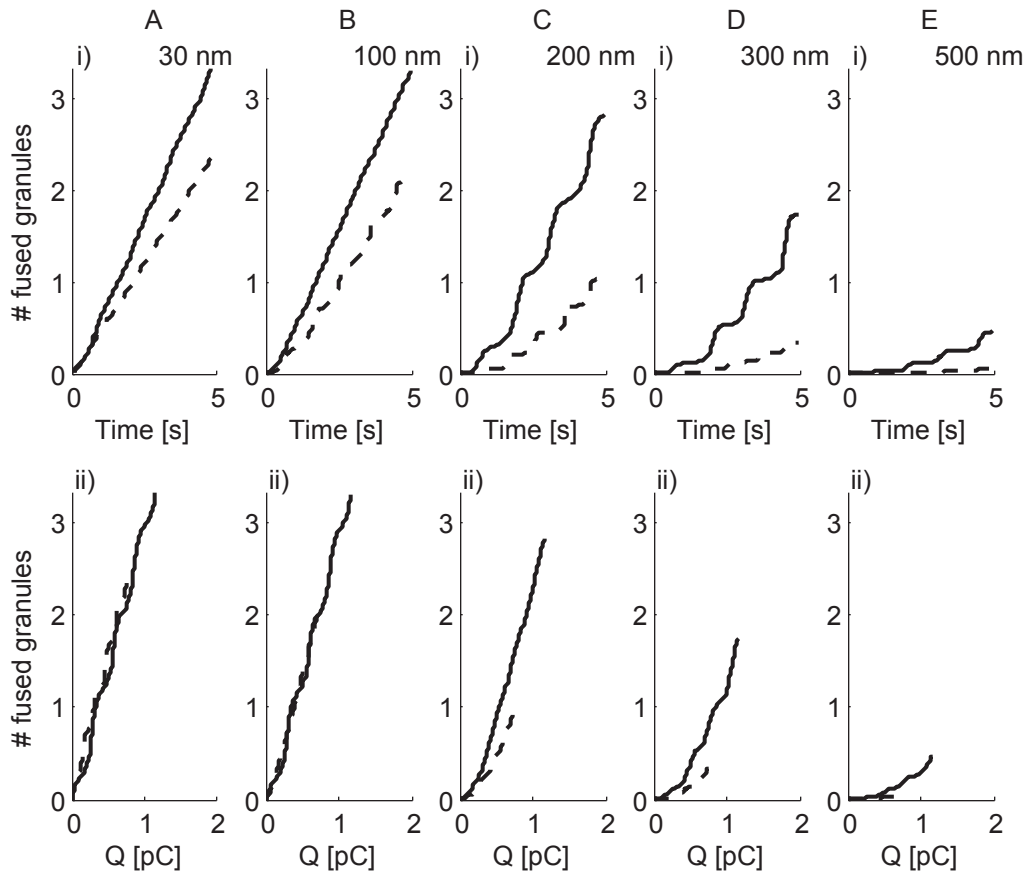
A
B
C
D
E
i)
30 nm
100 nm
200 nm
300 nm
500 nm
# fused granules
Time [s]
ii)
Q [pC]

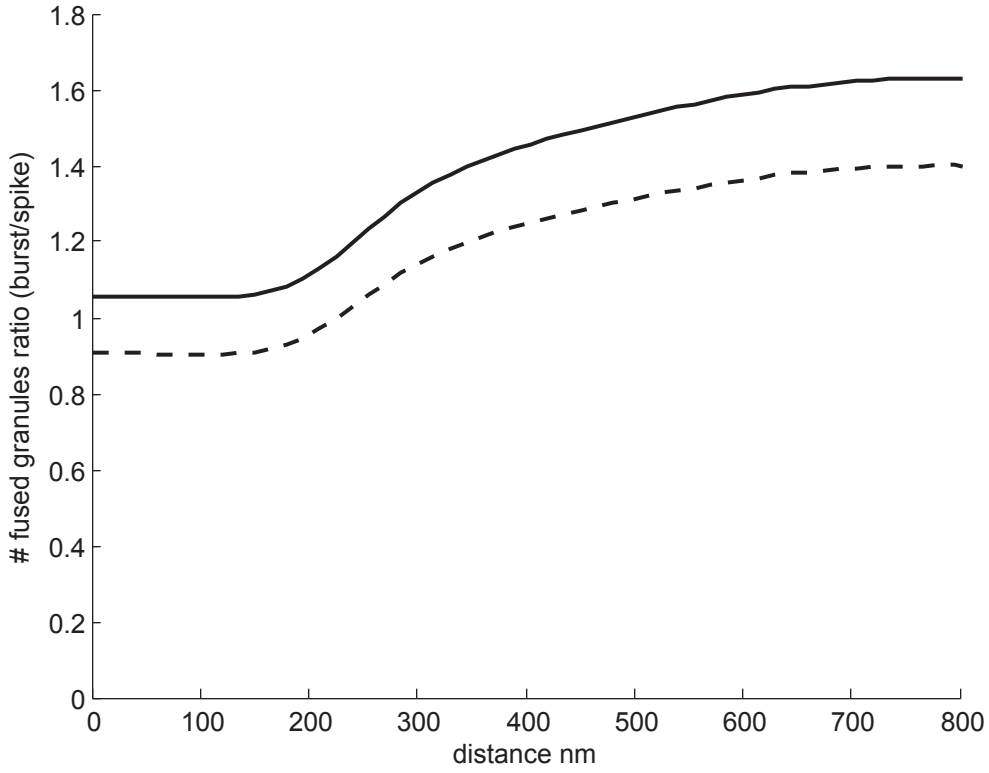
1.8
1.6
1.4
1.2
1
0.8
0.6
0.4
0.2
0
# fused granules ratio (burst/spike)
0
100
200
300
400
500
600
700
800
distance nm